crystals

MDPI

Article

Stabilizing Perovskite Solar Cells by Methyltriphenylphosphonium Iodide Studied with Maximum Power Point Tracking

Niklas Manikowsky [1,2,3], Zekarias Teklu Gebremichael [1,2,4], Chikezie Williams Ugokwe [1,2], Bashudev Bhandari [1,2,3], Steffi Stumpf [1,5], Ulrich S. Schubert [1,2,5] and Harald Hoppe [1,2,*]

1 Laboratory of Organic and Macromolecular Chemistry (IOMC Jena), Friedrich Schiller University Jena, 07743 Jena, Germany; niklas.manikowsky@uni-jena.de (N.M.); zekariasteklu.gebremichael@uni-jena.de (Z.T.G.); chikezie.ugokwe@uni-jena.de (C.W.U.); bashudev.bhandari@uni-jena.de (B.B.); steffi.stumpf@uni-jena.de (S.S.); ulrich.schubert@uni-jena.de (U.S.S.)
2 Center for Energy and Environmental Chemistry Jena (CEEC Jena), Friedrich Schiller University Jena, 07743 Jena, Germany
3 Faculty of Physics and Astronomy, Friedrich Schiller University Jena, 07743 Jena, Germany
4 College of Natural and Computational Science, Aksum University, Aksum P.O. Box 1010, Tigray Region, Ethiopia
5 Jena Center for Soft Matter (JCSM), Friedrich Schiller University Jena, 07743 Jena, Germany
* Correspondence: harald.hoppe@uni-jena.de

Abstract: The use of organic halide salts to passivate metal halide perovskite (MHP) surface defects has been studied extensively. Passivating the surface defects of the MHP is of critical importance for realizing highly efficient and stable perovskite solar cells (PSCs). Here, the successful application of a multifunctional organic salt, methyltriphenylphosphonium iodide (MTPPI), used as a passivation additive for grain boundary defects and as a molecular sealing layer in terms of stabilization, has been used to stabilize the mixed cation perovskite RbCsMAFA-PbIBr. To assess the passivating and stabilizing effects of MTPPI on RbCsMAFA-PbIBr PSCs, maximum power point tracking (MPPT) was applied as the most realistic and closest-to-application condition for the ageing test. Here, perovskite solar cells were aged under a light source yielding an excitation intensity corresponding to one sun with maximum power point tracking, which was interrupted periodically by current–voltage sweeps. This allowed for the extraction of all photovoltaic parameters necessary for a proper understanding of the ageing process. The MTPPI additive can donate iodine anions to halide vacancies and compensate a negative surface excess charge with cation interactions. On top of this, the large and bulky methyltriphenylphosphonium ($MTPP^+$) cation may block both the escape of volatile perovskite components and the ingress of oxygen and water vapour. These collective roles of MTPPI have improved both the efficiency and stability of the solar cells compared to the reference without passivation additives.

Keywords: perovskite; solar cell; passivation; stabilization; methyltriphenylphosphonium iodide (MTPPI); maximum power point tracking (MPPT)

check for updates

Academic Editor: Liangyao Chen

Received: 16 December 2024
Revised: 31 January 2025
Accepted: 5 February 2025
Published: 13 February 2025

Citation: Manikowsky, N.; Gebremichael, Z.T.; Ugokwe, C.W.; Bhandari, B.; Stumpf, S.; Schubert, U.S.; Hoppe, H. Stabilizing Perovskite Solar Cells by Methyltriphenylphosphonium Iodide Studied with Maximum Power Point Tracking. *Crystals* **2025**, *15*, 176. https://doi.org/10.3390/cryst15020176

Copyright: © 2025 by the authors. Licensee MDPI, Basel, Switzerland. This article is an open access article distributed under the terms and conditions of the Creative Commons Attribution (CC BY) license (https://creativecommons.org/licenses/by/4.0/).

1. Introduction

In recent years, photovoltaic devices based on hybrid metal halide perovskite solar cells (PSCs) have become a prominent research topic in the energy conversion field. These material systems have their own unique and vital properties that enable their use for photovoltaic applications. Ease of precursor solution preparation and fabrication processes, coupled with their tunable precursor compositions, tunable bandgap, high light absorption

coefficient, long charge carrier diffusion length, and broad optoelectronic applications are the factors that make PSCs the next leading generation in the photovoltaic field [1].

However, to unlock the full potential of PSCs in the photovoltaic industry, and to meet the market-desired lifetime expectation of 20–25 years [2], the issue of operational stability requires further attention [3].

While the record power conversion efficiency (PCE) of PSCs has reached 26.7% [4], the outlook for commercialization of PSCs remains limited due to multiple challenging degradation causes. For progressing the assessment of PSC device stabilization more effectively, it is useful to employ standardized, universally accepted protocols for stability testing and data dissemination [2,5,6]. Standardized ageing procedures have been defined and agreed upon under the International Summit on Organic Photovoltaic Stability (ISOS) testing protocols [2,5,6]. Maximum power point tracking (MPPT) is an ideal and advanced testing condition for metal halide perovskite-based solar cells (MH-PSC) because the voltage across the device is nearly constant and the operation is close to application levels. Already in 2018, running ISOS-protocols with continuous MPPT was demonstrated [7].

Most of today's MH-PSC ageing studies are focused on regulating crystal growth and optimizing interfacial properties in order to yield increased operational stability [8–23]. Crystal growth during device preparation is directly linked to the amount of interfaces, such as, respectively, grain boundaries, which are the sites at which the following processes limit, the performance, and the stability of MH-PSCs.

Firstly, the degradation pathways of perovskites naturally start at their grain boundaries because, here, either volatile components escape from—or reactive agents, such as moisture and oxygen, attack on—the perovskite. Both of these processes obviously result in the decomposition of the crystal [24–35]. Secondly, interfaces cause abrupt changes in the electronic properties, leading to trap-state formation and, consequently, enhanced charge carrier recombination [36–40], as well as photocurrent hysteresis due to trap-state occupation and the resulting ion migration [36,41,42]. Thus, grain boundaries cause a twofold problem: (i) immediate performance losses, and (ii) performance losses over time due to perovskite decomposition reactions.

In order to prevent and reduce charge carrier recombination through grain boundaries, electronic passivation strategies, following the ideas from classical solar cells, were introduced [43–48]. Since the interface or grain boundary represents an abrupt end of the ionic perovskite crystal, commonly uncompensated charges reside there, causing changes in electronic properties. These effects can be minimized by the compensation and delocalization of interfacial charge [49].

If charge compensation at the interfaces is combined with bulky organic molecules, decomposition reactions are discouraged, since neither the perovskite components can leave, nor the reactive agents can enter, the perovskite. Thus, the proper choice of passivating additives can provide both beneficial effects, namely reduced charge recombination as well as grain boundary sealing, and consequently yield improved performance and stability at the same time [49–54].

One prominent and popular approach is based on employing organic cations. Lee et al. have introduced the use of phenethylammonium cations (PEA^+) to effectively passivate the grain boundary defects of MAFA-based perovskite films [51]. They claim that the addition of PEA^+ resulted in both increased charge carrier lifetimes and moisture resistance in the unencapsulated devices. Currently, organic ammonium [52,55–59] and sulfonium [50,60–62] salt-passivating additives have become quite common tools to enhance stability and performance under different stress factors and ageing conditions [48,63].

It is obvious that, besides organic ammonium, organic phosphonium salts are also suitable for the same task of passivation. A motivation for using phosphonium instead of

ammonium salts may be found in the fact that phosphonium constitutes the larger cation. In fact, the first extended research study in using organic phosphonium salts was conducted as early as 2015 by Sun et al. [64]. The authors investigated two archetypical types, either (i) bulky tetraphenylphosphonium (TPP^+) or (ii) more linear tetrabutylphosphonium (TBP^+) cations. The second type was also employed as ammonium salt, but both turned out not to be as successful as the TPP^+, for which the halide anion was varied between Iodide (I), Chloride (Cl), and Bromide (Br). While—in contrast to TPPBr—the TPPCl-based devices also yielded a strong improvement in the fill factor over the reference, the best performance was found for TPPI. An influence on the kinetics of film formation, and thus crystallinity, may be due to differently sized Pb^{2+}-chelating I^-, Br^-, and Cl^- anions [64]. Due to the fact that TPPI can co-crystallize with PCBM, application of the same was also done by overcasting the organic salt on top of the PCBM electron extraction layer, yielding further performance increases, possibly due to doping [64]. The same research group demonstrated that the TPPCl can be used within the two-step synthesis of methylammoniumlead iodide (MAPI) by application on top of the lead iodide (PbI_2) precursor film [65]. Choubey et al. chose methyltriphenylphosphonium iodide (MTPPI) to passivate and stabilize n-i-p solar cells based on the fully inorganic $CsPbIBr_2$ perovskite [66]. By modifying the MTPPI concentration, the film and crystal morphology was strongly affected, which also resulted in a relative performance increase by about 50%. While only a slight increase in the photoluminescence (PL) intensity was found, a strong increase in recombination resistance was detected using electrochemical impedance spectroscopy (EIS), indicating reduced defects and improved contact with the adjacent carbon electrode. In another study, Chen et al. employed 3-carboxypropyl-triphenyl phosphonium bromide (3CPTPPBr), bearing a carboxylate-group at the end of a short aliphatic chain together with PCBA (a fullerene derivative) at the interface between the inorganic Titaniumoxide (TiO_2) layer and the perovskite film [67]. This treatment not only yielded an improvement in all photovoltaic (PV) parameters, but also resulted in a noticeably strong improvement in device stability under different ageing conditions. Recently, Liu et al. used TPPBr for the $CsPbIBr_2$ perovskite and demonstrated not only a performance increase, but also improved device stability over 700 h either in air or under higher temperatures [68]. Zhang et al. have demonstrated that tetrabutylphosphonium bromide (TBPBr) is also capable of passivating $CsPbBr_3$ perovskites [69]. This has been demonstrated by steady-state and time-resolved photoluminescence (TR-PL), as well as by transient absorption (TA). Finally, Azam et al. demonstrated defect passivation for methylammonium lead iodide (MAPI perovskite) by using TPPCl [70]. The authors demonstrated that, for concentrations of 1 mg TPPCl per millilitre, large grain sizes could be obtained, which was accompanied by increases in photocurrent, steady-state photoluminescence, and photovoltage by a reduction in the charge recombination. Furthermore, the authors showed that the surface of the perovskite become significantly more hydrophobic, supporting its stability.

Intrigued by the possibility of using phosphonium halides as alternative surface defect passivators on perovskite thin films, this study extends the application of methyltriphenylphosphonium iodide (MTPPI) as passivating additive for the mixed four cation RbCsMAFA-PbIBr perovskite absorber. Phosphonium salt was also chosen over ammonium salt to minimize the potential chemical interactions with the perovskite crystal [64]. This is because alkyl or aromatic ammonium cations can form hybrid structures of organic–inorganic layers with metal halides, which ultimately change the physical properties of the passivated perovskite thin film [71].

Likewise, the additive MTPPI may yield a stabilization effect via iodide ion donation and cation interactions. The iodide ions can fill potential halide vacancies, thus reducing defect states. On top of this, the large and bulky methyltriphenylphosphonium ($MTPP^+$)

cation can passivate surface trap states by interacting with halide ions, blocking mobile ion pathways.

2. Materials and Methods

2.1. Materials and Solution Preparation

For fabricating thin films and perovskite solar cell devices, various materials and solutions were used. Solvents such as isopropanol and toluene were purchased from VWR Chemicals (Germany, Darmstadt). Chlorobenzene (CB) was placed over a molecular sieve (≥99.5% (GC)). N,N-Dimenthylformamid (DMF) was extra dried over a molecular sieve (≥99.8% (GC)) and dimethylsulfoxid (DMSO) was extra dried over a molecular sieve (≥99.7% (GC)) supplied by Fisher Scientific GmbH (Germany, Schwerte). Furthermore, lead iodide (PbI_2), lead bromide ($PbBr_2$), cesium iodide (CsI) (Tokio Chemical Industry, Tokio, Japan, TCI), rubidium iodide (RbI) (Sigma Aldrich, Germany, Taufkirchen), formamidium iodide (FAI), and methylammonium bromide (MABr) (Dyesol, Germany, Munich) were used. PEDOT:PSS P VP AI 4083 was supplied by Heraeus Clevios GmbH (Germany, Leverkusen). Bathocuproin (BCP) (Alfa Aeasar GmbH, Germany, Karlsruhe); phenyl-C_{60}-butyric acid methyl ester (PCBM) (Solenne b.v.) and Copper pellets (Kurt J. Lesker Company, Dresden, Germany) were used. The passivation additive methyltriphenylphosphonium iodide (MTPPI) was synthesized in house by Maximilian Kleinsteuber (Germany, Dresden). The mass fraction (%) addition of MTPPI was varied between 0.025 wt.% and 0.2 wt.%, corresponding to a molar ratio of about 0.038%, up to about 0.3% mole of MTPPI, compared to the number of lead atoms.

For the precursor solution, the following solutions were prepared. An amount of 1.5 M of lead iodide (691.52 mg·mL^{-1}) and lead bromide (550.52 mg·mL^{-1}) were dissolved in DMF/DMSO 4:1 v/v. Furthermore, 1.5 M of cesium iodide (389.72 mg·mL^{-1}) and rubidium iodide (318.56 mg·mL^{-1}) were dissolved in DMSO, and were annealed together at 60 °C overnight.

For this work, the mixed four-cation perovskite RbCsMAFA was applied as an active layer, closely following the work by Saliba et al. [72].

The methylammonium bromide (MABr) and formamidinium iodide (FAI) powders were first weighed out in two separate vials. Then, 1.5M solution of PbI_2 ($PbBr_2$) in 4:1 v/v DMF:DMSO was added to the vials containing the FAI (MABr) powder to obtain a stoichiometry of FAI/PbI_2 (MABr/$PbBr_2$) of 1:1.09 (i.e., 9% lead excess) to obtain $FAPbI_3$ ($MAPbBr_3$). The $FAPbI_3$ and $MAPbBr_3$ were then mixed in a 5:1 v/v ratio to obtain the MAFA solution. CsMAFA was obtained by adding 5 vol% of 1.5M CsI to the MAFA solution. The RbCsMAFA precursor was finally prepared by adding 5 vol% of 1.5 M RbI solution to the CsMAFA precursor solution. Finally, RbCsMAFA-PbIBr has a nominal precursor solution composition of $(RbI)_{0.05}$ $[(CsI)_{0.05}$ $[(MA_{0.17}FA_{0.83})$ $Pb(I_{0.83}Br_{0.17})_3]_{0.95}]_{0.95}]$, which may be further adopted during crystallization. For further details, the interested reader is referred to the Supporting Information.

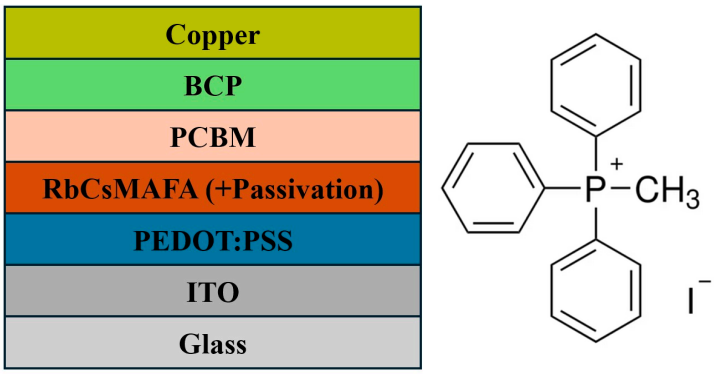
In order to ensure precise volumetric preparation, the pipettes used were calibrated using samples of the same solvents, and we compared their volume with their weights via the density of the solvents.

A 20 mg·mL^{-1} PCBM was dissolved in CB and kept at 60 °C overnight. Indium-doped tin oxide (ITO) pre-patterned substrates (Xinyan Technology Limited, 10 Ω cm^{-2}) were used as the cathode contact.

2.2. Film and Device Fabrication

The pre-patterned ITO/glass substrates were cleaned with cotton buds in toluene and sequentially further with toluene and isopropanol in an ultrasonicated bath at 40 °C

for 15 min each. Subsequently, the substrates were dried with N_2 stream and subjected to argon plasma cleaning for 5 min. The AI 4083 formulation of PEDOT:PSS was applied through a 0.45 µm PES filter and spin-coated for 35 s at 4000 rpm, yielding a film thickness of about 40 nm. Afterwards, the substrate was placed on a hot plate at 80 °C. Timing begins with the first substrate on the hot plate and ends after the last is coated. Once complete, the hot plate temperature was raised to 178 °C for 20 min. When finished, the substrates are immediately transferred to the glove box and cooled to room temperature for further processing. An amount of 100 µL of each variation in precursor solution were dropped onto the substrate and spin-coated for 3500 rpm for 35 s. The perovskite formation on the spin coater is modified by spilling the solvent chlorobenzene at 25 s remaining spin-time, and, finally, the sample is placed onto a hot plate at 100 °C for 30 min. This procedure yields film thicknesses of about 550–580 nm (see data in the SI for comparison). Subsequently, 100 µL of PCBM in CB is dropped onto the layer stack and spin-coated for 45 s at 1000 rpm, yielding about 62 nm film thickness. This layer stack is then transferred to the hot plate at 100 °C for 10 min. After patterning the area for the electrode, the substrate is placed at the evaporation mask and vacuum yielding 2.2×10^{-6} bar. 5 nm of BCP is first, and then 300 nm of copper are evaporated, controlled by the thickness monitor. The final layer stack for devices studied in here is glass/ITO/PEDOT:PSS/RbCsMAFA(+MTPPI)/PCBM/BCP/Cu (without encapsulation), and this is depicted in Scheme 1 together with the chemical structure of the passivation additive, MTPPI.



Scheme 1. Layer stack with its materials (**left**) and the chemical structure of methyltriphenylphosphonium iodide (MTPPI) (**right**), the passivation additive, are displayed.

2.3. Characterization

To analyze the perovskite film formation and corresponding performance, imaging, spectroscopic, solar cell performance, and stability characterization methods were used. For optical investigation, scanning electron microscopy (SEM) was performed with a Sigma VP Field Emission Scanning Electron Microscope (Carl-Zeiss AG, Oberkochen, Germany) using the InLens detector with an accelerating voltage of 8 kV to investigate the perovskite surface morphology of films as a function of different concentrations of MTPPI. Photoluminescence (PL) spectra were recorded with an Avantes AvaSpec ULS-2048X64 fibre spectrometer with 500 ms integration time and without further averaging. The PL intensity was corrected for the absorptance of the films at the wavelength of laser excitation (405 nm). UV/visible spectroscopy was conducted with two Avantes AvaSpec-ULS3648-USB2-UA-25 fibre spectrometers in order to gain insight into the transmittance and reflectance of perovskite films at 90°. This was performed with a 13 ms integration time and using two measurements for averaging. For the analyzing devices, a Keithley 2400 source measuring unit controlled using a computer along with a light-emitting diode (LED) solar simulator calibrated to yield an excitation density corresponding to one sun were used to measure the current–voltage (IV) characteristics of solar cell devices. For assessing

the stability of the devices, a novel maximum power point tracking (MPPT) system was used (purchased from Automatic Research GmbH, Nürnberg, Germany), employing a self-developed measurement routine. The MPPT was achieved by small variations over time in the driving voltage V and corresponding back measurements of the photocurrent I_P. Thus, the newly determined power output $P = I_P \times V$ can be compared with the old one, and the new MPP is set for the maximum of the two. The ageing setup yields a light excitation density corresponding to one sun when using constant LED illumination. The initial maximum power point (MPP) is determined by the average of the MPP assessment of the initial forward and backward current–voltage scans and corresponding photovoltaic parameter evaluations. Following the initial IV scans, the system is then tracking the MPP at all times, only to be interrupted for certain time intervals, when additional forward and reverse IV scans are conducted. For the current study, in the first 24 h, IV scans were conducted hourly; for the next 48 h, IV scans were recorded every 2 h and every 3 h thereafter, ranging between −0.7 and 2 V driving voltages. The short-circuit current I_{SC} and the open circuit voltage V_{OC} were obtained from the IV curve cutting the ordinate and the abscissa, respectively. The fill factor was obtained from the determination of the maximum power point and comparison with the product of I_{SC} and V_{OC}. The parallel R_P and series R_S resistances were obtained from the inverse gradients fitted to the IV curve at around 0 Volts and close to +2 Volts, considering at least 5–10 measurement points from the IV curve.

3. Results

In the following sections, the impact of using MTPPI as a processing and passivation agent for the RbCsMAFA-PbIBr perovskite is reported concerning its structural, optical, and photovoltaic properties. For this, three different mass concentrations of MTPPI were used in comparison to the MTPPI-free reference sample.

3.1. Structural and Optical Properties

3.1.1. Structural Properties by Scanning Electron Microscopy

Different film samples which had been processed on glass/PEDOT:PSS substrates were characterized using a field emission scanning electron microscope (FE-SEM). For the detection of the surface properties, the Inlens-detector and an acceleration voltage of 8 KV were used. The results are shown for comparison in Figure 1.

Upon closer inspection of Figure 1, it becomes noticeable that, with additional MTPPI content, the crystallites appear somewhat smaller on average. This is, in principle, an unwanted result, since smaller crystallites stand for more grain boundaries, which, in general, is a drawback for device performance and stability. However, as detailed in the Supplementary Information, after an initial drop, the average crystal size seems to increase for increasing MTPPI contents again. Since grain sizes remain below the reference even for the highest MTPPI concentration, an overcompensation of the increased area of grain boundaries by the electronic passivation effect is required. The information about the average crystal sizes and their standard deviation is given in Table 1.

Table 1. Overview of average perovskite crystal grain sizes determined from SEM images in Figure 1 as a function of varying MTPPI concentration.

MTPPI wt.%	Average Grain Size in nm	Std. Deviation in nm
0.00	269.5	27.07
0.05	235.6	24.67
0.10	237.6	15.47
0.20	257.1	16.55

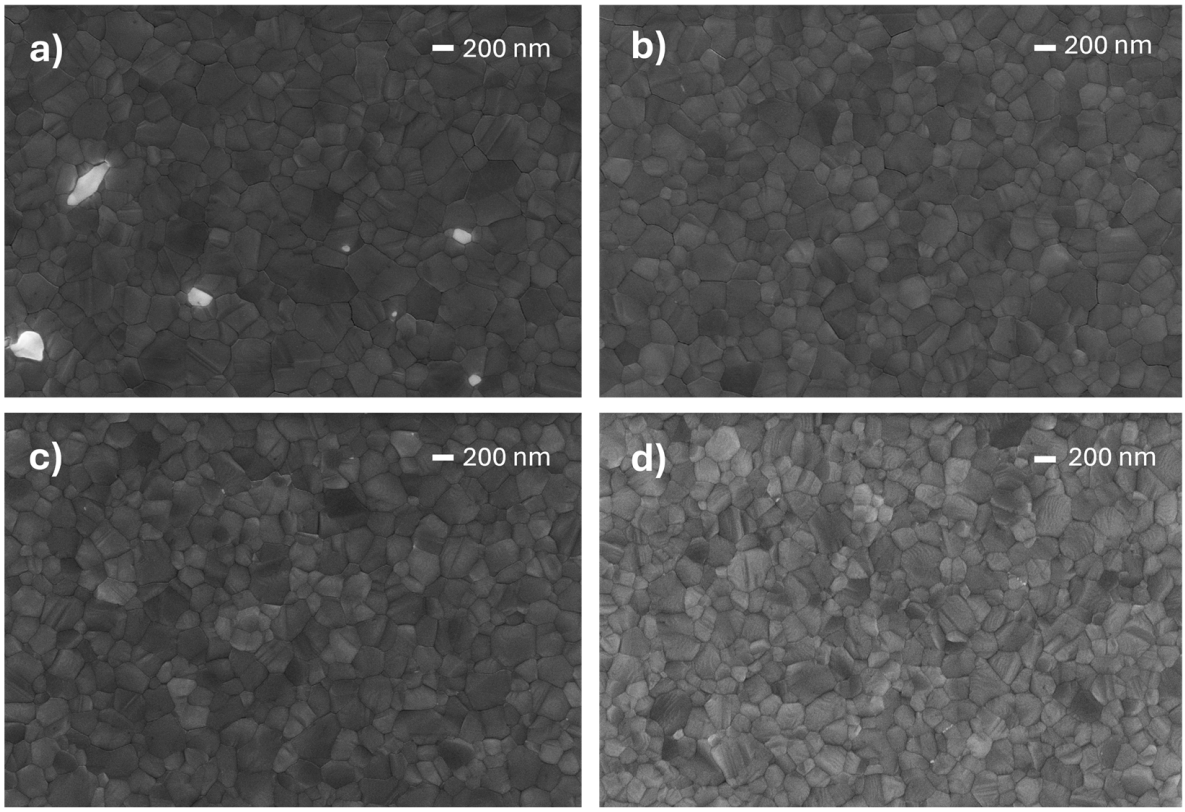


Figure 1. SEM images of four different multi-crystalline RbCsMAFA-PbIBr perovskite films (**a**) containing 0.00 wt.%, (**b**) containing 0.05 wt.%, (**c**) containing 0.10 wt.%, and (**d**) containing 0.20 wt.% of MTPPI additive. The scale bar represents a length of 200 nm. Note: the bright particles in section "(**a**)" are typical for pristine PbI_2 (compare with [73,74]).

3.1.2. Optical Properties by UV-Vis and Photoluminescence Spectroscopy

Furthermore, RbCsMAFA-PbIBr perovskite films bearing various MTPPI mass concentrations were spin-coated on top of PEDOT:PSS-coated glass substrates for optical investigations. First, UV-vis spectroscopy was used in order to record the transmittance and reflectance spectra and to compute the absorptance spectrum from those.

From Figure 2 it is obvious that the differences in transmittance, reflectance and absorptance are only minor in regions above the bandgap. Below the bandgap oscillations are generally being observed, which may hint towards interference effects within these layer stacks. It is noteworthy to mention that these oscillations differ significantly for the reference (or control) sample bearing no MTPPI additive. Thus, it cannot be ruled out that a subtle change in film thickness is obtained when using even smaller amounts of the MTPPI processing agent.

For the evaluation of the photoluminescence (PL), commonly differences in absorptance at the wavelength of the laser excitation (405 nm) are considered and corrected for. However, as mentioned above, there are almost no variations, and the absorptances are very close to each other. In stark contrast, the photoluminescence data exhibit large variations with the different amounts of MTPPI added (compare with Figure 3).

In fact, all PL spectra show a peak at about 763 nm, corresponding to the bandgap of this perovskite crystal. With increasing MTPPI mass concentration, the PL peak intensity rises strongly and superlinearly. While adding 0.05 wt.% of MTPPI did not remarkably change the PL intensity, enhancing the MTPPI concentration to the double (0.10 wt.%), also doubled the PL signal. Doubling the MTPPI concentration once more yields an increase in the PL signal by more than a factor of 5. Note that this happens even though the average

crystallite decreases in size and the total grain boundary area keeps increasing (compare with Figure 1).

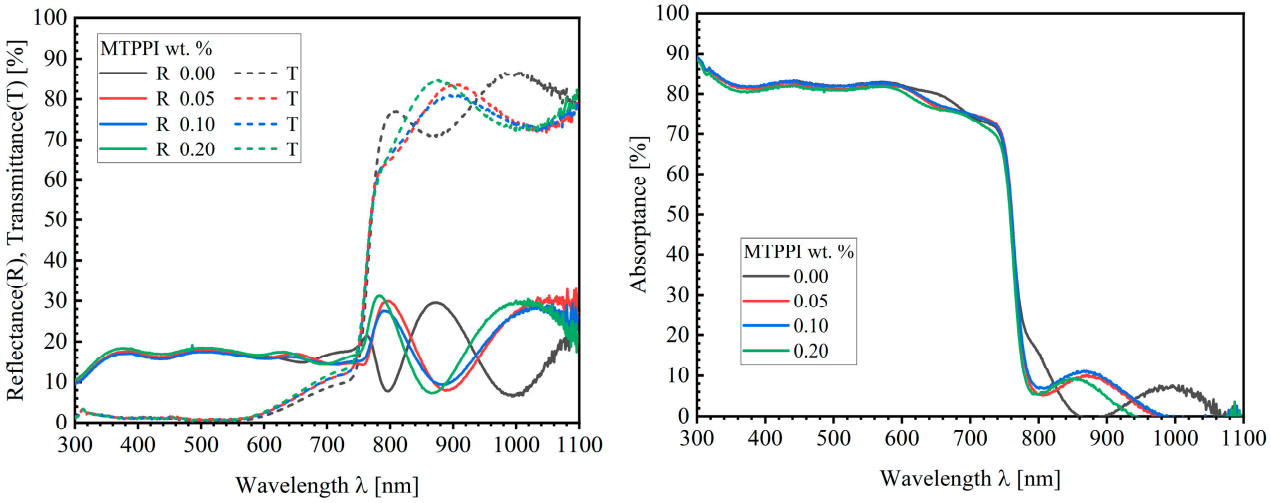


Figure 2. Transmittance, reflectance (both **left**), and absorptance (**right**) of RbCsMAFA-PbIBr perovskite films cast on PEDOT:PSS-coated glass substrates, bearing different amounts of MTPPI processing agent.

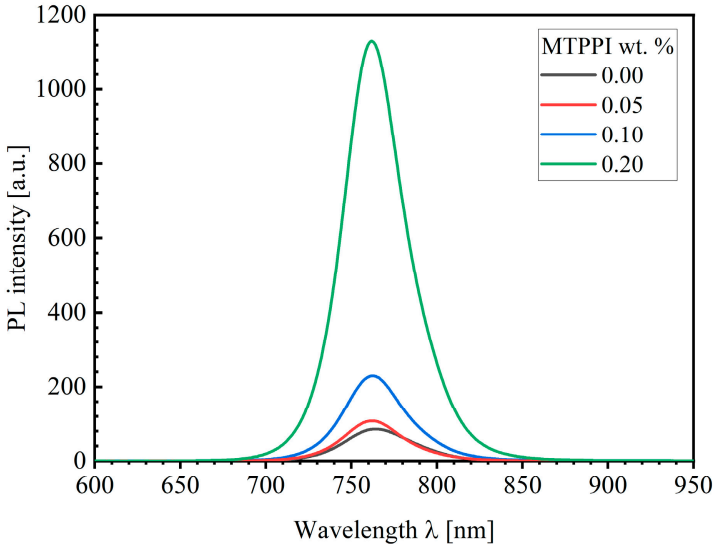


Figure 3. Photoluminescence (PL) intensity spectra for RbCsMAFA-PbIBr perovskite films showing virtually the same absorptance: with an increasing amount of MTPPI additive, the PL intensity was increasing superlinearly. The recovery of the radiative recombination is a strong indicator for the successful passivation of trap states, commonly located at the grain boundaries.

Since the strong increase in PL is a clear sign of the reduction in non-radiative recombination processes of charge carriers, it can already safely concluded that, indeed, MTPPI decreases the number of surface or grain boundary defects and thus displays a successful passivation. The remaining question, then, is whether this success can also be transferred into real solar cell devices.

3.2. Photovoltaic Properties: Performance and Stability

Photovoltaic solar cell devices were realized with photoactive layers stacked in between glass/ITO/PEDOT:PSS for hole and BCP/PCBM/Cu for electron extraction. A systematic variation in the MTPPI mass concentration was conducted, where, in this case, one additional value was tested with 0.025 wt.%. As compared to the reference device,

which had no MTPPI additive, all additive concentrations between 0.025 wt.% and 0.20 wt.% exhibited clear improvements in the solar cell device's performance (see Figure 4). While the JSC initially reduced slightly, the open circuit voltage jumped from an average value of about 875 to 950 mV for the smallest MTPPI concentration and kept increasing with higher MTPPI concentrations up to about 1025 mV. Such a close correlation of passivator concentration with open circuit voltage clearly confirms the success of reduced interfacial and grain boundary charge recombination. Accompanying the open circuit voltage increase, an increase in the parallel resistance, as well as in the fill factor, was observed. While the former increases gradually, the latter was immediately improved upon the smallest MTPPI addition by a more than 10% relative increase. Overall, the performance of the devices peaked at about 0.1 wt.% of MTPPI. However, the slight loss in performance for 0.2 wt.% MTPPI seems to be connected to a series resistance problem, which may be an indication that too much passivation material is deposited between the photoactive layer and the corresponding charge extraction layers.

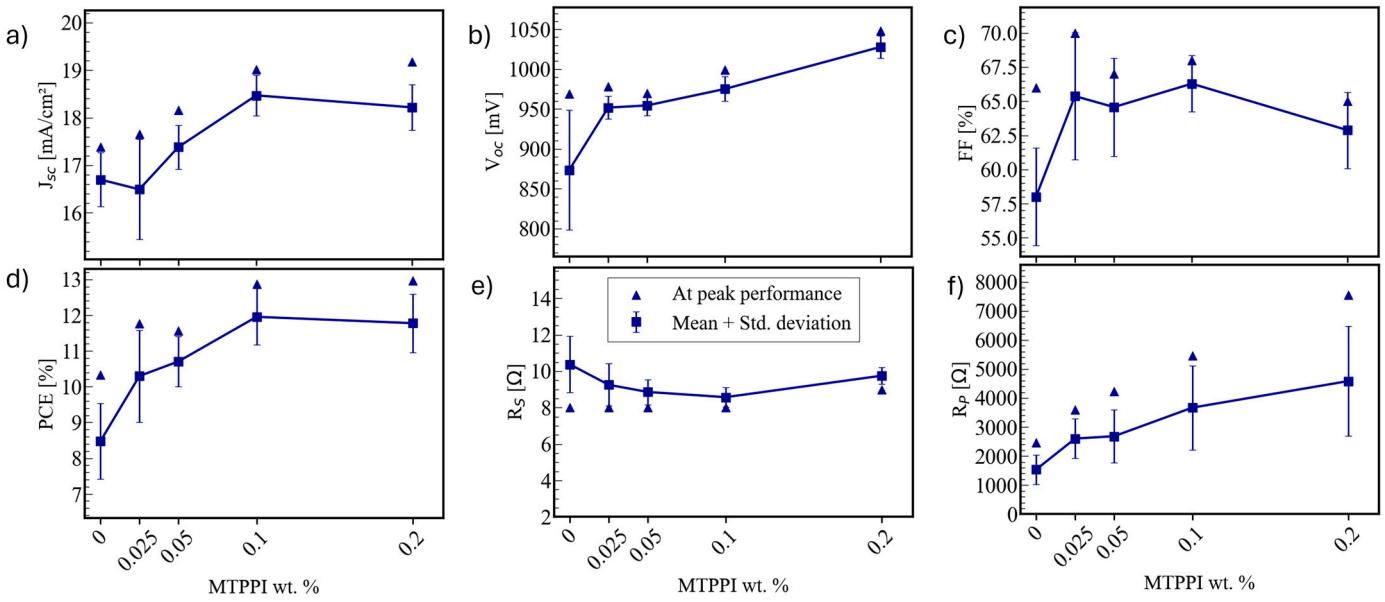


Figure 4. Photovoltaic parameters as a function of the MTPPI mass fraction. (**a**) Short circuit density, (**b**) open circuit voltage, (**c**) fill factor, (**d**) power conversion efficiency, (**e**) series resistance, (**f**) parallel resistance. The full lines indicate the trend for the averaged data—in this case, from 4 to 8 solar cells for each data point—while the closed triangle indicates the maximal value achieved. Clearly, the performance rises in increasing MTPPI mass fractions.

In order to cross-check the short circuit current density, external quantum efficiency measurements (see Figure 5) were recorded with a bias illumination, yielding an excitation density of about one sun.

For these sample devices, indeed, short circuit current densities overcoming those determined by IV characterization were obtained, and indeed the additive yielded a significant increase in the photocurrent compared to the reference device. The performance study revealed encouraging data and confirmed the passivation effect, with an optimum at 0.2 wt.% of MTPPI additive for the best devices (see Table 2). At this point, it remained to be investigated whether the second effect, namely the stabilization, could also be achieved.

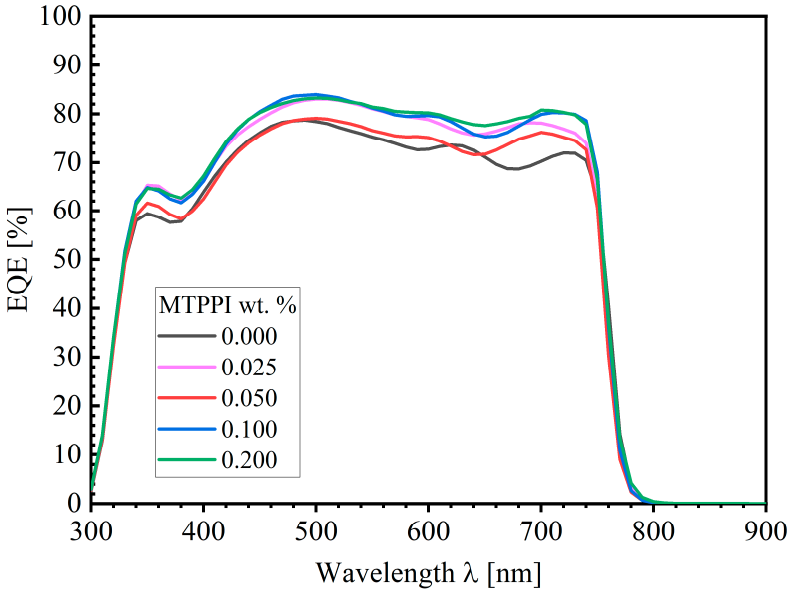


Figure 5. External quantum efficiency (EQE) spectra of the solar cells confirm a consistent increase in photocurrent with even small concentrations of MTPPI additive. The calculated total photocurrents for an AM 1.5G spectrum in fact yielded even higher values than the IV-characterization beforehand.

Table 2. Overview of photovoltaic parameters of best solar cell devices for each concentration of MTPPI additive. The via EQE-date corrected short circuit current and power conversion efficiency are also shown.

wt.%	J_{SC} [mA/cm^2]	$J_{SC,EQE}$ [mA/cm^2]	V_{OC} [mV]	FF [%]	PCE [%]	PCE_{EQE} [%]	Rs [Ω]	Rp [Ω]
0.000	17.09	17.99	918	66	10.34	10.88	11	2260
0.025	17.65	18.53	951	70	11.76	12.35	8	3150
0.050	18.15	17.61	951	67	11.56	11.22	9	1127
0.100	19.02	19.04	972	67	12.48	12.49	9	3896
0.200	19.18	19.11	1036	65	12.97	12.92	10	5139

For the ageing study, a subset of devices from the above performance study was used, simply due to the fact that the ageing setup could not take up each and every device. In this regard, the smallest MTPPI mass fraction was left out from the ageing study, as it seemed the least promising. Nevertheless, the reference without MTPPI was certainly part of this study. As described in the Materials and Methods section, the unsealed devices were aged within the glovebox under nitrogen atmosphere under continuous LED illumination, yielding an excitation density within the devices corresponding to one sun light intensity. Most of the time, the devices were kept at the maximum power point (MPPT), which was interrupted initially every single, then every second, and later every third hour for carrying out a forward and reverse IV sweep. The latter enabled us to extract the photovoltaic parameters over time, which will be discussed in the following section.

As expected from the beginning, all devices did show a strong degradation (see Figure 6). This is due to three facts: (i) the devices were unsealed, thus easing the loss of volatile components; (ii) the devices were continuously illuminated, providing no chance of light–dark regeneration cycles; and (iii) the devices were kept under maximum power point tracking (MPPT), providing another factor of continuous stress. Nevertheless, there is a considerable improvement in the rising mass fractions of the added MTPPI observed; while the reference device ended up with only ~0.4% final power conversion efficiency

(PCE), the device stabilized by 0.2 wt.% MTPPI showed the best stability, with a final PCE of about 1.6%.

The largest losses occurred for the short circuit photocurrents in all cases, while 0.1 and 0.2 wt.% MTPPI yielded nearly the same ageing curve. The next critical losses were observed for the fill factor, which were gradually less severe the more MTPPI was applied. In case of the open circuit voltage (V_{OC}) and the series resistance (R_S), a major difference was found for the reference device; this suffered even from remarkable losses for the V_{OC} and exhibited the strongest rise for the series resistance. All devices bearing MTPPI exhibited a remarkably stable series resistance. The parallel resistance (R_P) exhibited the strongest variations over time, which have to be connected with some abnormal IV characteristics. The latter is subject to ongoing research.

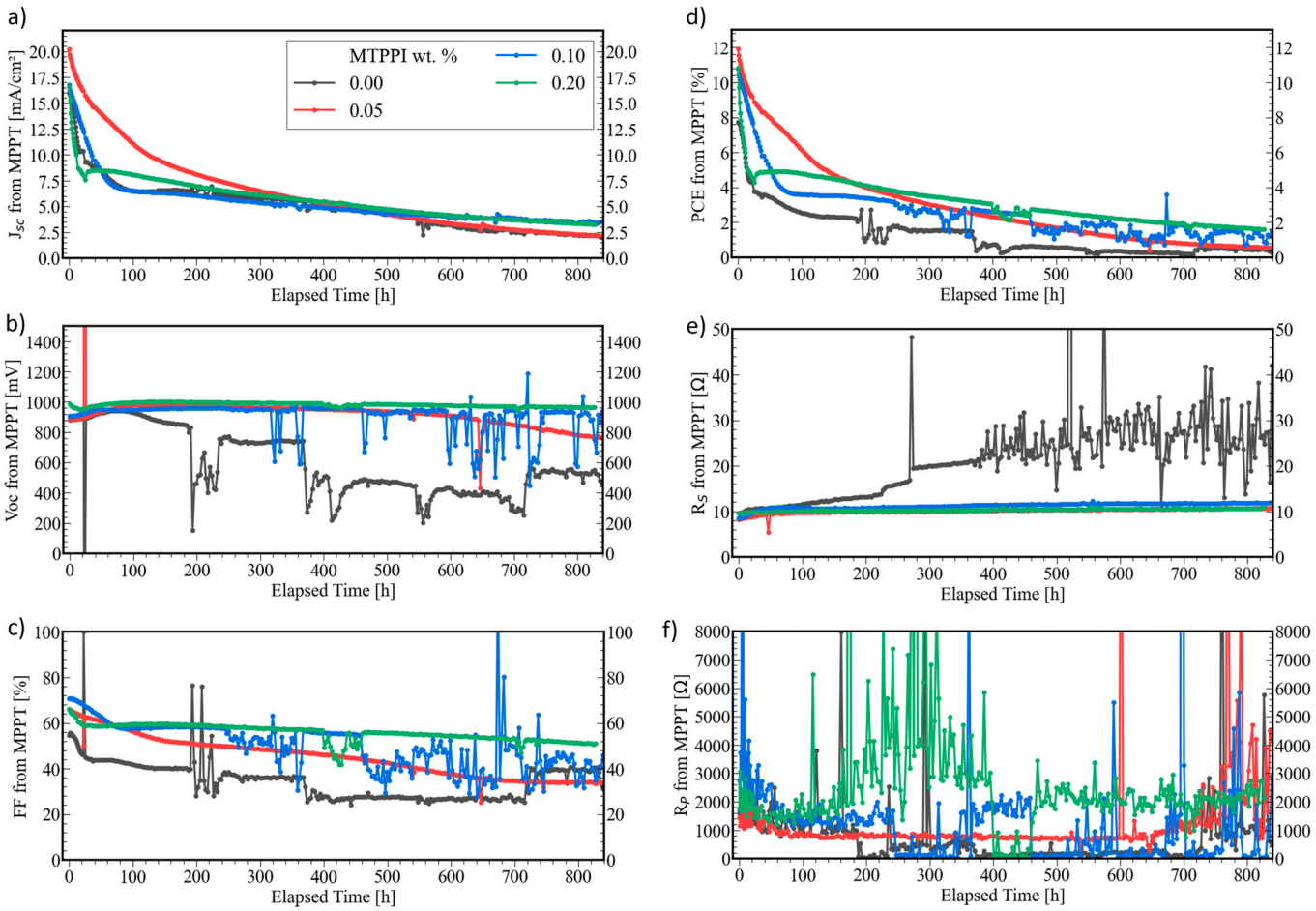


Figure 6. Summary of the ageing of unsealed devices under continuous illumination, being tracked at the maximum power point for more than 800 h inside the glovebox. While all devices show considerable degradation, the device containing 0.2 wt.% mass fraction of MTPPI exhibited a considerably improved stability. Shown are the (**a**) short-circuit photocurrents, (**b**) open circuit voltage, (**c**) fill factor, (**d**) power conversion efficiency, (**e**) series resistance, and (**f**) parallel resistance.

For visual inspection, Figure 7 displays the temporal development of the IV characteristics for the four different MTPPI concentrations. It is clearly visible that the highest concentration also yielded the most stable forward currents, while, in all cases, the photocurrent loss is the dominating factor for performance decay.

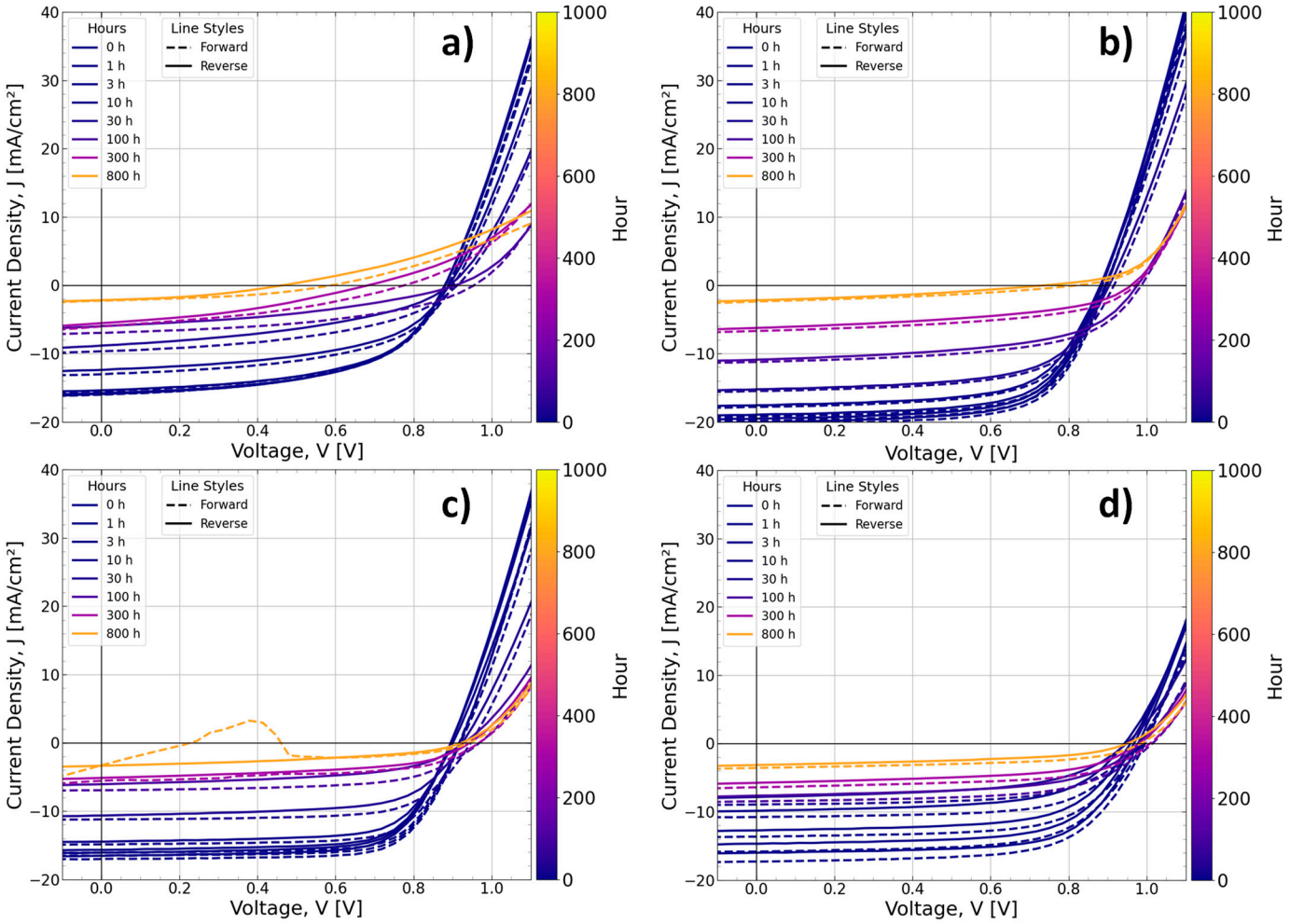


Figure 7. IV-characteristics of reverse IV-sweep development over time for increasing (from **top left** to **bottom right**) concentrations of MTPPI mass fractions (0.00, 0.05, 0.10, and 0.20 wt.%). While in all cases the photocurrent decrease is obvious, the forward currents remained nearly stable for the highest MTPPI concentration.

4. Discussion

While many materials bearing ammonium have been already employed for the passivation and stabilization of perovskite solar cells, phosphonium-based organic salts are still rare. In this study, MTPPI was successfully employed for that purpose. Used as a processing agent, MTPPI did, in fact, alter the film's morphology, being, respectively, the number, shape, and size of the crystallites of RbCsMAFA-PbIBr perovskite photoactive layer absorbers, as shown using SEM. The average crystallite unfortunately became smaller on average when increasing MTPPI, thereby increasing the grain boundary's (interfacial) area. However, the photoluminescence study clearly showed that higher MTPPI concentrations yielded strongly super-linear increases in the PL signal, indicating a successful passivation by preventing non-radiative recombination effects. This has been nicely confirmed by the solar cell investigations, in which a strong and sudden rise in the open circuit voltage could be found for all devices that contained an MTPPI additive. While the performance peaked for a 0.1 wt.% mass fraction of MTPPI, the stability was also improved, thus confirming the functionality of hindering the outgassing of volatile components.

5. Conclusions

Overall, this study demonstrates the successful use of a phosphonium salt for the passivation and stabilization of a perovskite absorber. However, the stability increase remained comparatively low, which may be related to continuous illumination, MPPT, and the fact that the devices were unsealed. Future research should therefore focus even more on preventing the volatile components of the perovskite from gassing out, improvements in the interfaces with charge-collecting layers, and possible reductions in hygroscopic components in the layer stack.

Supplementary Materials: The supporting information can be downloaded at: https://www.mdpi.com/article/10.3390/cryst15020176/s1.

Author Contributions: Conceptualization, N.M., C.W.U. and H.H.; Methodology, C.W.U. and H.H.; Formal analysis, C.W.U. and H.H.; Investigation, N.M., B.B. and S.S.; Resources, U.S.S. and H.H.; Writing—original draft, N.M., Z.T.G. and H.H.; Writing—review & editing, S.S., U.S.S. and H.H.; Supervision, H.H.; Project administration, H.H.; Funding acquisition, U.S.S. All authors have read and agreed to the published version of the manuscript.

Funding: VDI/VDE within the framework of 'Zentrales Innovationsprogramm Mittelstand (ZIM) des BMWK' for the Hidronik-Project 'Printed PV-Check', funding number 16KN098739. Thüringer Ministerium für Wirtschaft, Wissenschaft und Digitale Gesellschaft (TMWWDG) for funding the CEEC Jena (RIS3 Innovation Center). The SEM facilities of the Jena Center for Soft Matter (JCSM) were established with a grant from the Deutsche Forschungsgemeinschaft (DFG). eza Aliakbari for support in automated data evaluation, Andrea Dellith for the AFM thickness meas-urements, and Maximilian Kleinsteuber for providing the MTPPI additive material.

Data Availability Statement: Original measurement data is available upon reasonable request.

Acknowledgments: H.H. thankfully acknowledges the financial funding from VDI/VDE within the framework of 'Zentrales Innovationsprogramm Mittelstand (ZIM) des BMWK' for the Hidronik-Project 'Printed PV-Check', funding number 16KN098739. U.S.S. is grateful to the Thüringer Ministerium für Wirtschaft, Wissenschaft und Digitale Gesellschaft (TMWWDG) for funding the CEEC Jena (RIS3 Innovation Center). The SEM facilities of the Jena Center for Soft Matter (JCSM) were established with a grant from the Deutsche Forschungsgemeinschaft (DFG). We thankfully acknowledge Reza Aliakbari for support in automated data evaluation, Andrea Dellith for the AFM thickness measurements, and Maximilian Kleinsteuber for providing the MTPPI additive material.

Conflicts of Interest: The authors declare no conflicts of interest.

References

1. Rao, M.K.; Sangeetha, D.; Selvakumar, M.; Sudhakar, Y.; Mahesha, M. Review on persistent challenges of perovskite solar cells' stability. *Sol. Energy* **2021**, *218*, 469–491. [CrossRef]
2. Khenkin, M.V.; Katz, E.A.; Abate, A.; Bardizza, G.; Berry, J.J.; Brabec, C.; Brunetti, F.; Bulović, V.; Burlingame, Q.; Di Carlo, A. Consensus statement for stability assessment and reporting for perovskite photovoltaics based on ISOS procedures. *Nat. Energy* **2020**, *5*, 35–49. [CrossRef]
3. Chen, S.; Liu, N.; Xu, F.; Wei, G. Challenges and Strategies Toward Future Stable Perovskite Photovoltaics. *Sol. RRL* **2023**, *7*, 2300479. [CrossRef]
4. Green, M.A.; Dunlop, E.D.; Yoshita, M.; Kopidakis, N.; Bothe, K.; Siefer, G.; Hao, X.; Jiang, J.Y. Solar Cell Efficiency Tables (Version 65). *Prog. Photovolt. Res. Appl.* **2022**, *30*, 687–701. [CrossRef]
5. Reese, M.O.; Gevorgyan, S.A.; Jørgensen, M.; Bundgaard, E.; Kurtz, S.R.; Ginley, D.S.; Olson, D.C.; Lloyd, M.T.; Morvillo, P.; Katz, E.A. Consensus stability testing protocols for organic photovoltaic materials and devices. *Sol. Energy Mater. Sol. Cells* **2011**, *95*, 1253–1267. [CrossRef]
6. Roesch, R.; Faber, T.; von Hauff, E.; Brown, T.M.; Lira-Cantu, M.; Hoppe, H. Procedures and Practices for Evaluating Thin-Film Solar Cell Stability. *Adv. Energy Mater.* **2015**, *5*, 24. [CrossRef]
7. Köbler, H.; Neubert, S.; Jankovec, M.; Glažar, B.; Haase, M.; Hilbert, C.; Topič, M.; Rech, B.; Abate, A. High-Throughput Aging System for Parallel Maximum Power Point Tracking of Perovskite Solar Cells. *Energy Technol.* **2022**, *10*, 2200234. [CrossRef]

8. Bu, T.L.; Ono, L.K.; Li, J.; Su, J.; Tong, G.Q.; Zhang, W.; Liu, Y.Q.; Zhang, J.H.; Chang, J.J.; Kazaoui, S.; et al. Modulating crystal growth of formamidinium-caesium perovskites for over 200 cm^2 photovoltaic sub-modules. *Nat. Energy* **2022**, *7*, 528–536. [CrossRef]
9. Zhou, T.; Xu, Z.Y.; Wang, R.; Dong, X.Y.; Fu, Q.; Liu, Y.S. Crystal Growth Regulation of 2D/3D Perovskite Films for Solar Cells with Both High Efficiency and Stability. *Adv. Mater.* **2022**, *34*, 10. [CrossRef]
10. Song, X.; Wang, W.W.; Sun, P.; Ma, W.L.; Chen, Z.K. Additive to regulate the perovskite crystal film growth in planar heterojunction solar cells. *Appl. Phys. Lett.* **2015**, *106*, 5. [CrossRef]
11. Ahn, N.; Kang, S.M.; Lee, J.W.; Choi, M.; Park, N.G. Thermodynamic regulation of $CH_3NH_3PbI_3$ crystal growth and its effect on photovoltaic performance of perovskite solar cells. *J. Mater. Chem. A* **2015**, *3*, 19901–19906. [CrossRef]
12. Zhu, H.W.; Zhang, F.; Xiao, Y.; Wang, S.R.; Li, X.G. Suppressing defects through thiadiazole derivatives that modulate $CH_3NH_3PbI_3$ crystal growth for highly stable perovskite solar cells under dark conditions. *J. Mater. Chem. A* **2018**, *6*, 4971–4980. [CrossRef]
13. Yu, R.N.; Wu, G.Z.; Shi, R.; Ma, Z.W.; Dang, Q.; Qing, Y.Z.; Zhang, C.Y.; Xu, K.X.; Tan, Z.A. Multidentate Coordination Induced Crystal Growth Regulation and Trap Passivation Enables over 24% Efficiency in Perovskite Solar Cells. *Adv. Energy Mater.* **2023**, *13*, 10. [CrossRef]
14. Chen, M.Q.; Dong, X.Y.; Xin, Y.F.; Gao, Y.P.; Fu, Q.; Wang, R.; Xu, Z.Y.; Chen, Y.; Liu, Y.S. Crystal Growth Regulation of Ruddlesden-Popper Perovskites via Self-Assembly of Semiconductor Spacers for Efficient Solar Cells. *Angew. Chem. Int. Edit.* **2024**, *63*, 11. [CrossRef]
15. Guo, Y.L.; Sato, W.; Shoyama, K.; Halim, H.; Itabashi, Y.; Shang, R.; Nakamura, E. Citric Acid Modulated Growth of Oriented Lead Perovskite Crystals for Efficient Solar Cells. *J. Am. Chem. Soc.* **2017**, *139*, 9598–9604. [CrossRef] [PubMed]
16. Hwang, I.; Jeong, I.; Lee, J.; Ko, M.J.; Yong, K. Enhancing Stability of Perovskite Solar Cells to Moisture by the Facile Hydrophobic Passivation. *ACS Appl. Mater. Interfaces* **2015**, *7*, 17330–17336. [CrossRef] [PubMed]
17. Kim, M.; Motti, S.G.; Sorrentino, R.; Petrozza, A. Enhanced solar cell stability by hygroscopic polymer passivation of metal halide perovskite thin film. *Energy Environ. Sci.* **2018**, *11*, 2609–2619. [CrossRef]
18. Zhang, H.; Nazeeruddin, M.K.; Choy, W.C.H. Perovskite Photovoltaics: The Significant Role of Ligands in Film Formation, Passivation, and Stability. *Adv. Mater.* **2019**, *31*, 29. [CrossRef] [PubMed]
19. Yusoff, A.B.; Vasilopoulou, M.; Georgiadou, D.G.; Palilis, L.C.; Abate, A.; Nazeeruddin, M.K. Passivation and process engineering approaches of halide perovskite films for high efficiency and stability perovskite solar cells. *Energy Environ. Sci.* **2021**, *14*, 2906–2953. [CrossRef]
20. Bi, H.; Liu, B.B.; He, D.M.; Bai, L.; Wang, W.Q.; Zang, Z.G.; Chen, J.Z. Interfacial defect passivation and stress release by multifunctional KPF6 modification for planar perovskite solar cells with enhanced efficiency and stability. *Chem. Eng. J.* **2021**, *418*, 10. [CrossRef]
21. Yang, B.W.; Suo, J.J.; Di Giacomo, F.; Olthof, S.; Bogachuk, D.; Kim, Y.; Sun, X.X.; Wagner, L.; Fu, F.; Zakeeruddin, S.M.; et al. Interfacial Passivation Engineering of Perovskite Solar Cells with Fill Factor over 82% and Outstanding Operational Stability on n-i-p Architecture. *Acs Energy Lett.* **2021**, *6*, 3916–3923. [CrossRef] [PubMed]
22. Zhang, L.Q.; Cao, K.; Qian, J.; Huang, Y.; Wang, X.X.; Ge, M.R.; Shen, W.; Huang, F.; Wang, M.H.; Zhang, W.Z.; et al. Crystallization control and multisite passivation of perovskites with amino acid to boost the efficiency and stability of perovskite solar cells. *J. Mater. Chem. C* **2020**, *8*, 17482–17490. [CrossRef]
23. Naghadeh, S.B.; Luo, B.B.; Abdelmageed, G.; Pu, Y.C.; Zhang, C.; Zhang, J.Z. Photophysical Properties and Improved Stability of Organic-Inorganic Perovskite by Surface Passivation. *J. Phys. Chem. C* **2018**, *122*, 15799–15818. [CrossRef]
24. Li, B.B.; Li, Y.F.; Zheng, C.Y.; Gao, D.Q.; Huang, W. Advancements in the stability of perovskite solar cells: Degradation mechanisms and improvement approaches. *RSC Adv.* **2016**, *6*, 38079–38091. [CrossRef]
25. Sanehira, E.M.; de Villers, B.J.T.; Schulz, P.; Reese, M.O.; Ferrere, S.; Zhu, K.; Lin, L.Y.; Berry, J.J.; Luther, J.M. Influence of Electrode Interfaces on the Stability of Perovskite Solar Cells: Reduced Degradation Using MoO_x/Al for Hole Collection. *Acs Energy Lett.* **2016**, *1*, 38–45. [CrossRef]
26. Zhao, L.F.; Kerner, R.A.; Xiao, Z.G.; Lin, Y.H.L.; Lee, K.M.; Schwartz, J.; Rand, B.P. Redox Chemistry Dominates the Degradation and Decomposition of Metal Halide Perovskite Optoelectronic Devices. *Acs Energy Lett.* **2016**, *1*, 595–602. [CrossRef]
27. Wang, Q.; Chen, B.; Liu, Y.; Deng, Y.H.; Bai, Y.; Dong, Q.F.; Huang, J.S. Scaling behavior of moisture-induced grain degradation in polycrystalline hybrid perovskite thin films. *Energy Environ. Sci.* **2017**, *10*, 516–522. [CrossRef]
28. Yun, J.S.; Kim, J.; Young, T.; Patterson, R.J.; Kim, D.; Seidel, J.; Lim, S.; Green, M.A.; Huang, S.J.; Ho-Baillie, A. Humidity-Induced Degradation via Grain Boundaries of $HC(NH_2)_2PbI_3$ Planar Perovskite Solar Cells. *Adv. Funct. Mater.* **2018**, *28*, 8. [CrossRef]
29. Kwak, K.; Lim, E.; Ahn, N.; Heo, J.; Bang, K.; Kim, S.K.; Choi, M. An atomistic mechanism for the degradation of perovskite solar cells by trapped charge. *Nanoscale* **2019**, *11*, 11369–11378. [CrossRef] [PubMed]
30. Wygant, B.R.; Ye, A.Z.; Dolocan, A.; Vu, Q.; Abbot, D.M.; Mullins, C.B. Probing the Degradation Chemistry and Enhanced Stability of 2D Organolead Halide Perovskites. *J. Am. Chem. Soc.* **2019**, *141*, 18170–18181. [CrossRef] [PubMed]

31. Ge, Y.; Mu, X.L.; Lu, Y.; Sui, M.L. Photoinduced Degradation of Lead Halide Perovskite Thin Films in Air. *Acta Phys. Chim. Sin.* **2020**, *36*, 9. [CrossRef]
32. Guo, P.F.; Ye, Q.; Liu, C.; Cao, F.R.; Yang, X.K.; Ye, L.F.; Zhao, W.H.; Wang, H.Y.; Li, L.; Wang, H.Q. Double Barriers for Moisture Degradation: Assembly of Hydrolysable Hydrophobic Molecules for Stable Perovskite Solar Cells with High Open-Circuit Voltage. *Adv. Funct. Mater.* **2020**, *30*, 9. [CrossRef]
33. Khadka, D.B.; Shirai, Y.; Yanagida, M.; Miyano, K. Insights into Accelerated Degradation of Perovskite Solar Cells under Continuous Illumination Driven by Thermal Stress and Interfacial Junction. *ACS Appl. Energ. Mater.* **2021**, *4*, 11121–11132. [CrossRef]
34. Sun, K.; Guo, R.J.; Liang, Y.X.; Heger, J.E.; Liu, S.P.; Yin, S.S.; Reus, M.A.; Spanier, L.V.; Deschler, F.; Bernstorff, S.; et al. Morphological Insights into the Degradation of Perovskite Solar Cells under Light and Humidity. *ACS Appl. Mater. Interfaces* **2023**, *15*, 30342–30349. [CrossRef] [PubMed]
35. Kore, B.P.; Jamshidi, M.; Gardner, J.M. The impact of moisture on the stability and degradation of perovskites in solar cells. *Mater. Adv.* **2024**, *5*, 2200–2217. [CrossRef]
36. Sherkar, T.S.; Momblona, C.; Gil-Escrig, L.; Avila, J.; Sessolo, M.; Bolink, H.J.; Koster, L.J.A. Recombination in Perovskite Solar Cells: Significance of Grain Boundaries, Interface Traps, and Defect Ions. *Acs Energy Lett.* **2017**, *2*, 1214–1222. [CrossRef] [PubMed]
37. Khadka, D.B.; Shirai, Y.; Yanagida, M.; Miyano, K. Degradation of encapsulated perovskite solar cells driven by deep trap states and interfacial deterioration. *J. Mater. Chem. C* **2018**, *6*, 162–170. [CrossRef]
38. Park, J.S.; Calbo, J.; Jung, Y.K.; Whalley, L.D.; Walsh, A. Accumulation of Deep Traps at Grain Boundaries in Halide Perovskites. *Acs Energy Lett.* **2019**, *4*, 1321–1327. [CrossRef]
39. Jia, P.C.; Qin, L.; Zhao, D.; Tang, Y.; Song, B.; Guo, J.H.; Li, X.M.; Li, L.; Cui, Q.H.; Hu, Y.F.; et al. The Trapped Charges at Grain Boundaries in Perovskite Solar Cells. *Adv. Funct. Mater.* **2021**, *31*, 8. [CrossRef]
40. Zheng, Y.T.; Li, Y.R.; Zhuang, R.S.; Wu, X.Y.; Tian, C.C.; Sun, A.X.; Chen, C.; Guo, Y.S.; Hua, Y.; Meng, K.; et al. Towards 26% efficiency in inverted perovskite solar cells via interfacial flipped band bending and suppressed deep-level traps. *Energy Environ. Sci.* **2024**, *17*, 1153–1162. [CrossRef]
41. Chen, Y.C.; Shi, J.; Li, X.T.; Li, S.Q.; Lv, X.D.; Sun, X.N.; Zheng, Y.Z.; Tao, X. A universal strategy combining interface and grain boundary engineering for negligible hysteresis and high efficiency (21.41%) planar perovskite solar cells. *J. Mater. Chem. A* **2020**, *8*, 6349–6359. [CrossRef]
42. Liu, J.; Yin, X.T.; Guo, Y.X.; Que, M.D.; Chen, J.; Chen, Z.; Que, W.X. Influence of Hole Transport Layers/Perovskite Interfaces on the Hysteresis Behavior of Inverted Perovskite Solar Cells. *ACS Appl. Energ. Mater.* **2020**, *3*, 6391–6399. [CrossRef]
43. Schulz, P.; Cahen, D.; Kahn, A. Halide Perovskites: Is It All about the Interfaces? *Chem. Rev.* **2019**, *119*, 3349–3417. [CrossRef] [PubMed]
44. Chen, J.Z.; Park, N.G. Materials and Methods for Interface Engineering toward Stable and Efficient Perovskite Solar Cells. *Acs Energy Lett.* **2020**, *5*, 2742–2786. [CrossRef]
45. Vasilopoulou, M.; Fakharuddin, A.; Coutsolelos, A.G.; Falaras, P.; Argitis, P.; Yusoff, A.R.B.; Nazeeruddin, M.K. Molecular materials as interfacial layers and additives in perovskite solar cells. *Chem. Soc. Rev.* **2020**, *49*, 4496–4526. [CrossRef]
46. Li, Y.H.; Xie, H.B.; Lim, E.L.; Hagfeldt, A.; Bi, D.Q. Recent Progress of Critical Interface Engineering for Highly Efficient and Stable Perovskite Solar Cells. *Adv. Energy Mater.* **2022**, *12*, 31. [CrossRef]
47. Isikgor, F.H.; Zhumagali, S.; Merino, L.V.T.; De Bastiani, M.; McCulloch, I.; De Wolf, S. Molecular engineering of contact interfaces for high-performance perovskite solar cells. *Nat. Rev. Mater.* **2023**, *8*, 89–108. [CrossRef]
48. Zhang, J.D.; Tang, S.C.; Zhu, M.Q.; Li, Z.H.; Cheng, Z.B.; Xiang, S.C.; Zhang, Z.J. The Role of Grain Boundaries in Organic-Inorganic Hybrid Perovskite Solar Cells and its Current Enhancement Strategies: A Review. *Energy Environ. Mater.* **2024**, *7*, 30. [CrossRef]
49. Zhang, H.; Pfeifer, L.; Zakeeruddin, S.M.; Chu, J.; Grätzel, M. Tailoring passivators for highly efficient and stable perovskite solar cells. *Nat. Rev. Chem.* **2023**, *7*, 632–652. [CrossRef]
50. Suo, J.; Yang, B.; Mosconi, E.; Bogachuk, D.; Doherty, T.A.; Frohna, K.; Kubicki, D.J.; Fu, F.; Kim, Y.; Er-Raji, O.; et al. Multifunctional sulfonium-based treatment for perovskite solar cells with less than 1% efficiency loss over 4500-h operational stability tests. *Nat. Energy* **2024**, *9*, 172–183. [CrossRef]
51. Lee, D.S.; Yun, J.S.; Kim, J.; Soufiani, A.M.; Chen, S.; Cho, Y.; Deng, X.; Seidel, J.; Lim, S.; Huang, S. Passivation of grain boundaries by phenethylammonium in formamidinium-methylammonium lead halide perovskite solar cells. *ACS Energy Lett.* **2018**, *3*, 647–654. [CrossRef]
52. Zhuang, J.; Mao, P.; Luan, Y.; Yi, X.; Tu, Z.; Zhang, Y.; Yi, Y.; Wei, Y.; Chen, N.; Lin, T.; et al. Interfacial passivation for perovskite solar cells: The effects of the functional group in phenethylammonium iodide. *ACS Energy Lett.* **2019**, *4*, 2913–2921. [CrossRef]
53. Yang, Y.M. Surface passivation of perovskite film for efficient solar cells. *J. Semicond.* **2019**, *40*, 040204-040204-2.
54. Yang, Z.; Chen, J.; Li, M.; Qi, M.; Zhang, G.; Chen, R.; Hu, J.; Liu, X.; Qin, C.; Xiao, L. 4-Methoxy phenethylammonium halide salts for surface passivation of perovskite films towards efficient and stable solar cells. *Chem. Eng. J.* **2024**, *494*, 152955. [CrossRef]

55. Liu, Y.N.; Duan, J.J.; Zhang, J.K.; Huang, S.M.; Wei, O.Y.; Bao, Q.Y.; Sun, Z.; Chen, X.H. High Efficiency and Stability of Inverted Perovskite Solar Cells Using Phenethyl Ammonium Iodide-Modified Interface of NiO_x and Perovskite Layers. *ACS Appl. Mater. Interfaces* **2020**, *12*, 771–779. [CrossRef]
56. Ye, Q.F.; Ma, F.; Zhao, Y.; Yu, S.Q.; Chu, Z.M.; Gao, P.Q.; Zhang, X.W.; You, J.B. Stabilizing γ-$CsPbI_3$ Perovskite via Phenylethylammonium for Efficient Solar Cells with Open-Circuit Voltage over 1.3 V. *Small* **2020**, *16*, 7. [CrossRef]
57. Zhang, F.; Huang, Q.X.; Song, J.; Zhang, Y.H.; Ding, C.; Liu, F.; Liu, D.; Li, X.B.; Yasuda, H.; Yoshida, K.; et al. Growth of Amorphous Passivation Layer Using Phenethylammonium Iodide for High-Performance Inverted Perovskite Solar Cells. *Sol. RRL* **2020**, *4*, 8. [CrossRef]
58. Meng, H.G.; Li, X.H.; Mai, Y.X.; Zhang, P.T.; Li, S.J. Enhanced Efficiency and Stability of Triple-Cation Perovskite Solar Cells through Engineering of the Cell Interface with Phenylethylammonium Thiocyanate. *ACS Appl. Mater. Interfaces* **2024**, *16*, 69430–69438. [CrossRef]
59. Qi, J.; Zhao, Y.; Zhang, X.W.; Yang, X.L.; Chen, Y.; Chu, Z.; Ye, Q.F.; Li, X.X.; Yin, Z.G.; You, J.B. Surface Passivation of Perovskite Film for Efficient Solar Cells. *Nat. Photonics* **2019**, *13*, 460–466.
60. Wu, T.H.; Ono, L.K.; Yoshioka, R.; Ding, C.F.; Zhang, C.Y.; Mariotti, S.; Zhang, J.H.; Mitrofanov, K.; Liu, X.; Segawa, H.; et al. Elimination of light-induced degradation at the nickel oxide-perovskite heterojunction by aprotic sulfonium layers towards long-term operationally stable inverted perovskite solar cells. *Energy Environ. Sci.* **2022**, *15*, 4612–4624. [CrossRef]
61. Zuo, X.; Kim, B.; Liu, B.B.; He, D.M.; Bai, L.; Wang, W.Q.; Xu, C.Y.; Song, Q.L.; Jia, C.Y.; Zang, Z.G.; et al. Passivating buried interface via self-assembled novel sulfonium salt toward stable and efficient perovskite solar cells. *Chem. Eng. J.* **2022**, *431*, 10. [CrossRef]
62. Kim, Y.; Lee, H.; Lee, C.; Kim, B.; Kwon, N.; Son, T.; Lee, J.H.; Sin, J.; Shin, T.; Yang, J.; et al. Enhancing performance of two-step fabricated perovskite solar cells with sulfonium triflate-based additive. *EcoMat* **2024**, *6*, 13. [CrossRef]
63. Girish, K. Advances in surface passivation of perovskites using organic halide salts for efficient and stable solar cells. *Surf. Interfaces* **2021**, *26*, 101420.
64. Sun, C.; Xue, Q.; Hu, Z.; Chen, Z.; Huang, F.; Yip, H.-L.; Cao, Y. Phosphonium Halides as Both Processing Additives and Interfacial Modifiers for High Performance Planar-Heterojunction Perovskite Solar Cells. *Small* **2015**, *11*, 3344–3350. [CrossRef]
65. Qi, J.; Yao, X.; Xu, W.; Wu, X.; Jiang, X.; Gong, X.; Cao, Y. Efficient Perovskite Solar Cells with Reduced Photocurrent Hysteresis through Tuned Crystallinity of Hybrid Perovskite Thin Films. *ACS Omega* **2018**, *3*, 7069–7076. [CrossRef]
66. Choubey, A.; Perumal, N.; Muthu, S.P.; Perumalsamy, R. Ambient-air fabrication of efficient and stable carbon-based inorganic perovskite solar cell based on $CsPbIBr_2$ film via organic salt passivation. *Sol. Energy* **2022**, *245*, 265–277. [CrossRef]
67. Chen, Z.; Li, Y.; Liu, Z.; Shi, J.; Yu, B.; Tan, S.; Cui, Y.; Tan, C.; Tian, F.; Wu, H.; et al. Reconfiguration toward Self-Assembled Monolayer Passivation for High-Performance Perovskite Solar Cells. *Adv. Energy Mater.* **2023**, *13*, 2202799. [CrossRef]
68. Liu, B.-Y.; Yang, H.-M.; Zuo, Y.-D.; Tao, Z.-H.; Li, J.-C.; Chang, Y.-J.; Tong, G.-Q.; Jiang, Y. Intermediate phase-assisted growth of $CsPbBr_3$ for high performance of carbon-based perovskite solar cells. *Rare Met.* **2024**, *43*, 2222–2229. [CrossRef]
69. Zhang, W.; Zheng, J.; Huang, W.; Zhao, M.; Jiang, B.; Bian, H.; Fang, Y. Revealing Mechanisms and Ultrafast Dynamics of Tetrabutyl Phosphonium Bromide Ionic Liquids Post-Treatment in $CsPbBr_3$ Perovskite Films. *J. Phys. Chem. C* **2024**, *128*, 1147–1155. [CrossRef]
70. Azam, M.; Ke, Z.; Luo, J.; Wan, Z.; Hassan, A.; Jia, C. Additive engineering enabled non-radiative defect passivation with improved moisture-resistance in efficient and stable perovskite solar cells. *Chem. Eng. J.* **2024**, *483*, 149424. [CrossRef]
71. Cheng, Z.; Lin, J. Layered organic–inorganic hybrid perovskites: Structure, optical properties, film preparation, patterning and templating engineering. *CrystEngComm* **2010**, *12*, 2646–2662. [CrossRef]
72. Saliba, M.; Correa-Baena, J.-P.; Wolff, C.M.; Stolterfoht, M.; Phung, N.; Albrecht, S.; Neher, D.; Abate, A. How to Make over 20% Efficient Perovskite Solar Cells in Regular (n–i–p) and Inverted (p–i–n) Architectures. *Chem. Mater.* **2018**, *30*, 4193–4201. [CrossRef]
73. Kalasariya, N.; Alexander, A.; Bhunia, P.K.; Gutierrez-Partida, E.; Benny, R.; Stolterfoht, M.; Namboothiry, M.A.G. Controlling Lead Halide Residue in Perovskite Solar Cells: A Method to Improve the Photostability and Hysteresis. *Sol. RRL* **2024**, *8*, 2300788. [CrossRef]
74. Jacobsson, T.J.; Correa-Baena, J.-P.; Halvani Anaraki, E.; Philippe, B.; Stranks, S.D.; Bouduban, M.E.F.; Tress, W.; Schenk, K.; Teuscher, J.; Moser, J.-E.; et al. Unreacted PbI2 as a Double-Edged Sword for Enhancing the Performance of Perovskite Solar Cells. *J. Am. Chem. Soc.* **2016**, *138*, 10331–10343. [CrossRef]

Disclaimer/Publisher's Note: The statements, opinions and data contained in all publications are solely those of the individual author(s) and contributor(s) and not of MDPI and/or the editor(s). MDPI and/or the editor(s) disclaim responsibility for any injury to people or property resulting from any ideas, methods, instructions or products referred to in the content.